izational energy than step 1 and is thus expected to be faster.

No appreciable transient absorption changes ($\tau \geq 30$ ns) are observed in laser flash photolysis of the one-electron-oxidized forms. It should be remarked that the spectra of intermediates of the type of that shown in Figure 7 are expected to be similar (except for small shifts on the order of 0.1–0.2 μm^{-1}) to those of the corresponding ground states. The most plausible explanation of the observed lack of spectral changes, however, is that the charge recombination (step 3), despite of the low exergonicity, is in the nanosecond or subnanosecond range. This conclusion is consistent with the kinetic parameters for the back-recombination reaction (step 3) that can be estimated from the spectral characteristics of the IT bands.[62,74]

Conclusions

It has been shown that the stepwise synthesis of discrete oligomeric complexes containing $Ru(bpy)_2^{2+}$ chromophoric units linked together by cyanide bridges is feasible. These complexes can be considered as pseudohomopolynuclear, in the sense that they are made up of identical building blocks connected, however, by asymmetric bridges. Indeed, their behavior is deeply influenced by the asymmetry of the bridges connecting the chromophoric units. In particular, it has been shown that (i) the more easily oxidizable Ru(II) centers in the polynuclear complexes are those that contain the greater number of N-bonded cyanides, (ii) the lowest MLCT excited state is always localized on the $Ru(bpy)_2^{2+}$ unit that has the greater number of N-bonded cyanides, and (iii) very efficient intramolecular energy transfer takes place from all the $Ru(bpy)_2^{2+}$ chromophoric units to that having the lowest excited state. Partial oxidation of these species gives rise to strong intervalence bands in the near-infrared region, indicating a relatively large degree of electron delocalization (relative to typical class II mixed-valence behavior).

These results are of some general interest, in particular with regard to the synthesis and the properties of more extended, polymeric structures of the same type. The possibility to direct intramolecular energy and electron transfer by taking advantage of the asymmetry in the bridging ligands seems to be particularly interesting in this regard.

Acknowledgment. This work was supported by the Ministero della Pubblica Istruzione and by the Consiglio Nazionale delle Ricerche (Progetto Finalizzato Chimica Fine e Secondaria II).

Registry No. $(2,2)PF_6$, 123165-05-9; $(2,2')PF_6$, 123099-59-2; $(2,2,2)(PF_6)_2$, 123099-63-8; $(2,3)(PF_6)_2$, 123099-65-0; $(2,3')(PF_6)_2$, 123099-67-2; $(2,3,2)(PF_6)_3$, 123099-69-4; $Ru(bpy)_2(NO_2)(CN)$, 123099-54-7; $Ru(phen)_2(NO_2)(CN)$, 123099-55-8; $[Ru(phen)_2(NO)(NO_2)](PF_6)_2$, 31450-89-2; $[Ru(bpy)_2(NO)(CN)](PF_6)_2$, 121176-17-8; $[Ru(phen)_2(NO)(CN)](PF_6)_2$, 123099-57-0; $Ru(bpy)_2(CN)_2$, 20506-36-9; $[Ru(phen)_2(CH_3OH)(CN)]PF_6$, 123099-61-6; $Ru(bpy)_2Cl_2$, 19542-80-4; $Ru(phen)_2(CN)$, 112087-85-1; $[NCRu(bpy)_2CNPt(dien)](ClO_4)_2$, 88360-14-9; $[(dien)PtNCRu(bpy)_2CNPt(dien)](ClO_4)_4$, 88377-85-9; $Ru(bpy)_2(CH_3OH)(NO_2)^+$, 47637-64-9.

(74) For example, using $\epsilon_{max} = 10000\ M^{-1}\ cm^{-1}$, $\nu_{max} = 0.80\ \mu m^{-1}$, and $\Delta\nu_{1/2} = 0.35\ \mu m^{-1}$ as experimental spectroscopic parameters, $\Delta G = 0.25$ eV as a reasonable driving force value and $\nu_N = 1 \times 10^{10}\ s^{-1}$ as a plausible (mainly outer-sphere) frequency factor, one obtains from standard equations[62] a calculated rate constant value of $4 \times 10^{10}\ s^{-1}$ for the back-recombination step in the mixed-valence binuclear complexes.

Contribution from the Department of Chemistry and Biochemistry, University of California, Los Angeles, California 90024

Quantitative Evaluation of the Relationships between Excited-State Geometry and the Intensities of Fundamentals, Overtones, and Combination Bands in Resonance Raman Spectra

Kyeong-Sook Kim Shin and Jeffrey I. Zink*

Received February 14, 1989

The factors that govern the resonance Raman intensities of fundamentals, overtones, and combination bands are quantitatively evaluated. The calculations and interpretation are based on the time-dependent theory of Lee, Tannor, and Heller. From the time-dependent point of view, the Raman intensities are governed by the overlap of the time-dependent wave packet with the final Raman wave function of interest as a function of time. The most important factors are the magnitude of the overlap and the time development of the overlap. The magnitudes of the overlaps for overtones of a given mode are smaller than that for its fundamental, and the magnitude for a combination band is smaller than those of the fundamentals of the modes comprising the combination band. Thus, the overtone and combination bands are weaker than fundamentals. The time development of the overlap depends on both the frequency of the vibration and the displacement of the excited potential surface relative to the ground potential surface along the normal coordinate. The damping of the overlap determines whether short-time or long-time processes dominate the intensities. For large molecules where short-time processes dominate, the larger the initial overlap and the faster the overlap increases with time, the higher the Raman intensity. The intensities of fundamentals, overtone bands, and combination bands will be discussed in terms of the overlap. Qualitative rules for interpreting excited-state molecular properties from the Raman intensities are developed. The spectra of $W(CO)_5$(pyridine) and $Rh_2(O_2CCH_3)_4L_2$, where L = PPh_3 or $AsPh_3$, are analyzed.

1. Introduction

Resonance Raman spectroscopy is frequently considered to be a complicated and esoteric method of obtaining vibrational spectra. However, the time-dependent theory of Lee, Tannor, and Heller shows that it is closely akin to absorption spectroscopy.[1-4] In addition, the new point of view shows that the intensity of a peak in a Raman spectrum provides detailed information about the excited-state potential surface along the normal mode giving rise to the peak.[5-8]

The purpose of this paper is to examine resonance Raman intensities from the time-dependent theoretical point of view in order to state general, qualitative rules for interpreting excited-state

(1) Lee, S.-Y.; Heller, E. J. *J. Chem. Phys.* **1979**, *71*, 4777.
(2) Heller, E. J. *Acc. Chem. Res.* **1981**, *14*, 368.
(3) Heller, E. J.; Sundberg, R. L.; Tannor, D. *J. Phys. Chem.* **1982**, *86*, 1822.
(4) Tannor, D.; Heller, E. J. *J. Chem. Phys.* **1982**, *77*, 202.
(5) Williams, S. O.; Imre, D. G. *J. Phys. Chem.* **1988**, *92*, 3363.
(6) Yoo, C. S.; Zink, J. I. *Inorg. Chem.* **1983**, *22*, 2474.
(7) Yang, Y. Y.; Zink, J. I. *Inorg. Chem.* **1985**, *24*, 4012.
(8) Myers, A. B.; Mathies, R. A.; Tannor, D. J.; Heller, E. J. *J. Chem. Phys.* **1982**, *77*, 3857.

0020-1669/89/1328-4358$01.50/0

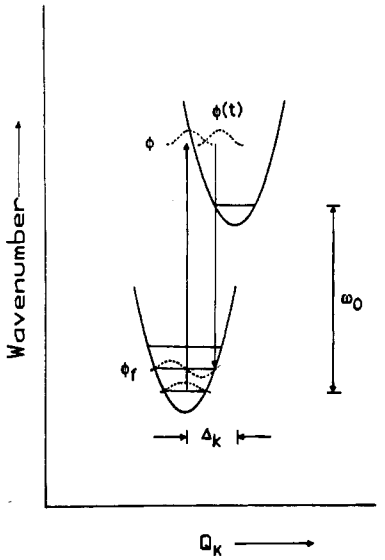

Figure 1. Illustration of the time-dependent theory of resonance Raman scattering. ϕ is the initial wave packet, $\phi(t)$ is the moving wave packet, ϕ_f is the final state of interest, and Δ_k is the displacement of the upper potential surface along the normal coordinate Q_k.

molecular properties from the Raman intensities. The intensities of not only the fundamentals but also those of overtone and combination bands are treated. The intensities are discussed in terms of the Raman excitation profiles, of which a slice at a given excitation wavenumber gives the Raman spectrum at that particular excitation wavenumber. Throughout this paper the goal will be to think in the time domain in order to understand the molecular properties governing the excitation profiles and/or spectra in the frequency domain.

In this paper, the important factors that govern the Raman intensities are identified and interpreted. The physical insight obtained from the time-dependent picture is emphasized. The intensities of fundamental, overtone, and combination bands are discussed in terms of the ground- and excited-state potential surfaces. Two specific calculations are carried out by using the time-dependent theory and are compared to experimental results. First, the theory is applied to the 18-mode fundamental spectrum of $W(CO)_5(py)$ (py = pyridine). In this example, the intensities of 18 fundamental modes are calculated. The distortions in the ^3E excited state[9,10] are determined and compared to those that were previously implicated in the missing mode effect (MIME).[11-14] Second, the calculation of the spectra of $Rh_2(O_2CCH_3)_4L_2$, where L = PPh_3 or $AsPh_3$, which contains fundamentals, overtones, and combination bands, is carried out. The distortions of nine (L = PPh_3) and six (L = $AsPh_3$) modes in the $^1A_{2u}$ excited state[15,16] are determined.

2. Theory

The time-dependent theory of Lee, Tannor, and Heller offers a new viewpoint of resonance Raman spectroscopy. It emphasizes the connection between potential surfaces, dynamics, and the spectroscopic observables. In addition, the computations are very efficient.

The Raman scattering cross section is given by[4]

$$\alpha_{fi} = \frac{i}{\hbar}\int_0^\infty \langle\phi_f|\phi(t)\rangle \exp[i(\omega_i + \omega_I)t - \Gamma t]\, dt \qquad (1)$$

where $|\phi_f\rangle = \mu|\chi_f\rangle$ is the final vibrational state, χ_f, of the ground electronic surface multiplied by the transition electric dipole moment, μ, $|\phi(t)\rangle = \exp(-iH_{ex}t/\hbar)|\phi\rangle$ is a moving wave packet propagated by the excited-state Hamiltonian, $|\phi\rangle = \mu|\chi\rangle$ is the initial vibrational state of the ground electronic surface multiplied by the electronic transition moment, Γ is the damping factor, $\hbar\omega_i$ is the zero-point energy of the ground electronic surface, and $\hbar\omega_I$ is the energy of the incident radiation.

The resonance Raman scattering amplitude is governed by the motion of a wave packet on a multidimensional hypersurface representing the excited electronic state potential. A cross section of a multidimensional surface along one of the normal modes that will be used to discuss the theory is shown in Figure 1.

The initial wavepacket, ϕ, makes a vertical transition onto the potential surface of the excited state, which, in general, is displaced relative to that of the ground state. The wave packet is not a stationary state and evolves according to the time-dependent Schrödinger equation. The quantity of interest is the overlap of the moving wave packet $\phi(t)$ with the final state of interest ϕ_f. ϕ_f is characterized by the normal mode k with vibrational quantum number n_k. If it is assumed that (a) the potential surfaces are harmonic, (b) the normal coordinates are not mixed in the excited state, (c) the transition dipole moment, μ, is constant, and (d) the force constants do not change in the excited state, then the overlap has the simple form

$$\langle\phi_f|\phi(t)\rangle = \prod_k \left\{ \exp\left[-\frac{\Delta_k^2}{2}(1 - \exp(-i\omega_k t)) - \frac{i\omega_k t}{2} \right] \times (1 - \exp(-i\omega_k t))^{n_k} \frac{(-1)^{n_k}\Delta_k^{n_k}}{(2^{n_k} n_k!)^{1/2}} \right\} \exp(-i\omega_0 t) \qquad (2)$$

In eq 2, ω_0 is the energy of the zero–zero electronic transition (E_{00}) in cm^{-1}, ω_k and Δ_k are respectively the wavenumber in cm^{-1} and the displacement of the kth normal mode, and n_k is the vibrational quantum number of the kth normal mode in the ground electronic state (n_k = 0, 1, 2, etc.). Equation 2 is composed of two parts. The exponential term in brackets is the kernel of absorption (A), and the other term is the Raman factor (R). The contribution of each part to the overlap for the Raman scattering will be discussed later. Equation 2 is used to calculate the cross sections for the fundamentals, overtones, and combination tones. For example, in order to calculate the cross section of the combination band $\nu_1 + \nu_2$ in a three-mode case, $n_1 = 1$, $n_2 = 1$, and $n_3 = 0$.

The harmonic approximation is not a requirement of time-dependent theory. It is used in this paper because the number of parameters to be fit is reduced and because in addition it allows the simple expression for the overlap (eq 2) to be used.

The Raman scattering cross section in the frequency domain is the half Fourier transform of the overlap in the time domain as shown in eq 1. The Raman intensity $I_{i\to f}$ into a particular mode f is

$$I_{i\to f} \propto \omega_I \omega_s^3 |\alpha_{fi}|^2 \qquad (3)$$

where ω_s is the frequency of the scattered radiation.

3. Spectral Features and Interpretation in the Time Domain

The observables in a Raman spectrum are the frequencies and the intensities of the scattered light. The most intense peaks are usually scattering by the fundamentals of the modes whose potential surfaces are most likely displaced in the resonant excited state. However, in resonance Raman spectra one or more overtones of a given mode are commonly found with significant intensities. In addition, combination bands involving two (or infrequently more) modes are sometimes found. The purpose of this section is to interpret the intensities of all of these features in terms of the ground-state and resonant excited-state potential surfaces. The time-dependent theory provides a physical interpretation of the dynamic processes on these potential surfaces which lead to the observed intensities. The three quantities in eq 1 and 2 that are used in the calculation (Δ_k, the displacement, ω_k, the vibrational frequency, and Γ, the damping factor) are individually and collectively discussed. The experimentally determined frequencies of the vibrational modes of $Rh_2(O_2CCH_3)_4(PPh_3)_2$ are used as the example in the following discussion.[17]

A. Fundamentals. Effect of Δ. The effect of the displacement, Δ, of the excited potential surface relative to the ground potential surface on the Raman intensities of fundamentals is considered in this section. The displacements are expressed in dimensionless

(9) Geoffroy, G. L.; Wrighton, M. S. *Organometallic Photochemistry*; Academic Press: New York, 1979.
(10) Dahlgren, R. M.; Zink, J. I. *Inorg. Chem.* **1977**, *16*, 3154.
(11) Tutt, L.; Tannor, D.; Heller, E. J.; Zink, J. I. *Inorg. Chem.* **1982**, *21*, 3858.
(12) Tutt, L.; Tannor, D.; Schindler, J.; Heller, E. J.; Zink, J. I. *J. Phys. Chem.* **1983**, *87*, 3017.
(13) Tutt, L.; Zink, J. I. *J. Am. Chem. Soc.* **1986**, *108*, 5830.
(14) Zink, J. I. *Coord. Chem. Rev.* **1985**, *64*, 93.
(15) Bursten, B. E.; Cotton, F. A. *Inorg. Chem.* **1981**, *20*, 3042.
(16) Sowa, T.; Kawamura, T.; Shida, T.; Yonezawa, T. *Inorg. Chem.* **1983**, *22*, 56.
(17) Clark, R. J. H.; Hempleman, A. J. *Inorg. Chem.* **1988**, *27*, 2225.

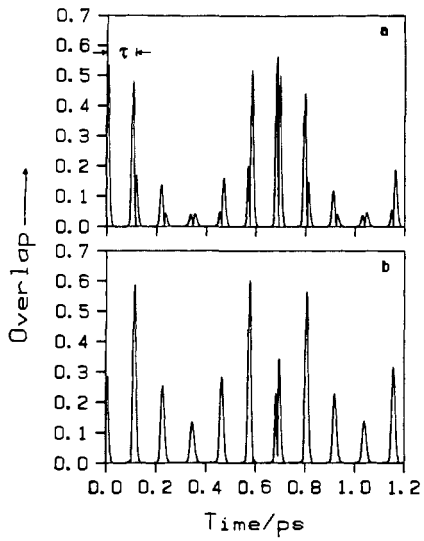

Figure 2. Magnitude of overlap versus time for (a) ν_1 and (b) ν_2. Γ = 0, ν_1 = 289 cm^{-1}, Δ_1 = 3.73, ν_2 = 338 cm^{-1}, and Δ_2 = 1.70. Time τ is one vibrational period.

units.[18] Although the absolute intensities can be measured and compared to the calculated intensities, in practice it is much more convenient and common to compare the relative intensities of the modes to each other or to an internal standard. The former comparisons will be used here.

The physical meaning of eq 1–3 is illustrated by using a two-mode example. In order to focus on the effect of Δ on the intensity, two modes that are similar in frequency and different in displacement are chosen. The displacement is 3.73 for ν_1 (289 cm^{-1}) and 1.70 for ν_2 (338 cm^{-1}).

The magnitude of the overlap, $|\langle\phi_f|\phi(t)\rangle|$ (eq 2), which is needed to calculate the Raman scattering intensities is plotted in Figure 2a for ν_1 (n_1 = 1, n_2 = 0, k = 2) and in Figure 2b for ν_2 (n_1 = 0, n_2 = 1, k = 2). A damping factor of zero is used in each plot. At time zero, ϕ makes a vertical transition to the upper surface. The overlaps $|\langle\phi_f|\phi(t)\rangle|$ at t = 0 are identically zero because ϕ and ϕ_f are orthogonal eigenstates. However, ϕ is not an eigenfunction of the upper surface and begins to evolve on the upper surface according to the time-dependent Schrödinger equation. There is a peak in the plot of $|\langle\phi_f|\phi(t)\rangle|$ versus time after $\phi(t)$ has moved away from the F–C region. This maximum is followed by a decrease as $\phi(t)$ moves further away. At still longer times, $\phi(t)$ will return to its initial position. At time τ after one vibrational period $\phi(t)$ and ϕ_f are once again orthogonal and $|\langle\phi_f|\phi(t)\rangle|$ drops to zero. Each return is responsible for an additional peak, resulting in a total of two maxima in $|\langle\phi_f|\phi(t)\rangle|$ as the wave packet goes from and comes back to its initial position. The classical turning point falls between these maxima. In the frequency domain (the excitation profile), the vibronic spacing ω is equal to $2\pi/\tau$.

The intensity of a Raman peak at a given excitation wavenumber ω_l is related to the area under the curve in the overlap versus time plot. However, only the overlap in the short-time region of the plot will be important in determining the Raman spectra of large molecules in condensed media because the damping factor is always nonzero. For example, when the damping factor is 300 cm^{-1}, most of the recurrences die and the first peak will be the dominant factor governing the Raman intensity. In this case, the more highly displaced the mode, the faster the initial increase in overlap, the smaller the effect of the damping, and the larger the intensity in the spectrum. When the damping factor is smaller (50 cm^{-1}, for example) the second and third recurrences will still have appreciable magnitude. In this case, the Raman intensity of ν_2 can be larger than that of ν_1 at certain excitation wavenumbers (vide infra). Details of the effect of the damping factor on the Raman intensities of the fundamental bands are discussed below.

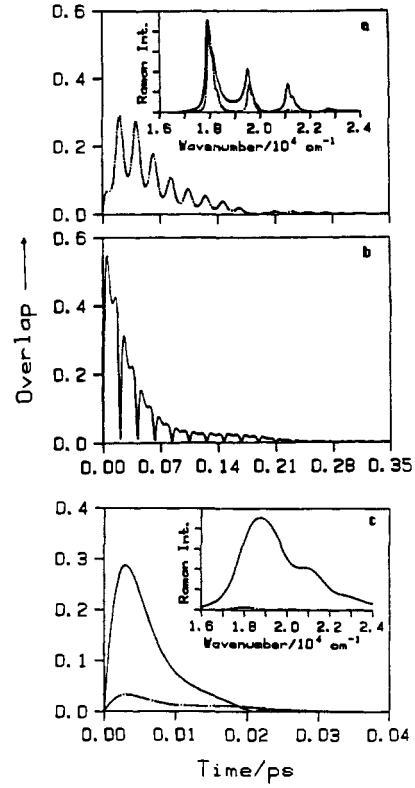

Figure 3. Magnitude of overlap versus time for (a) ν_{10} (176 cm^{-1}, Δ = 1.0, –·–) and (b) ν_9 (1588 cm^{-1}, Δ = 1.0, —) when the damping factor is 100 cm^{-1} (inset to (a) shows the excitation profiles of ν_9 (—) and ν_{10} (–·–) when the damping factor is 100 cm^{-1} and E_{00} is 17 950 cm^{-1}) and (c) ν_{10} (176 cm^{-1}, Δ = 1.0, –·–) and ν_9 (1588 cm^{-1}, Δ = 1.0, —) when the damping factor is 1000 cm^{-1} (inset shows the excitation profiles of ν_9 (—) and ν_{10} (–·–) when the damping factor is 1000 cm^{-1} and E_{00} is 17 950 cm^{-1}).

The Raman intensity of a given mode increases as the displacement increases when the damping factor is large enough such that recurrences at long times are damped out and the overlap at short times dominates. In the absence of damping, no simple rule can be stated because the intensity can change drastically with a small change in the incident frequency. The Raman intensity for a highly displaced mode in a large molecule in a condensed medium is larger than that of a mode with a small displacement not because the overlap itself is larger but because significant overlap occurs faster in time.

Effect of Vibrational Frequency. The effect of the frequency of a vibrational mode, ω_i, on its Raman intensity relative to a second mode ω_j is considered in this section. In order to emphasize the effect of the frequency, two modes with very different frequencies, 1588 cm^{-1} (ν_9) and 176 cm^{-1} (ν_{10}), are chosen. The displacements of both of these modes are set equal to 1.0.

The plots of the magnitude of the overlap versus time for ν_{10} (–·–) and ν_9 (—) are shown in parts a and b, respectively, of Figure 3. As the wave packet begins to move, the magnitude of the overlap for the high-frequency mode increases faster in time than that for the low-frequency mode because the slope of the potential surface for the high-frequency mode is steeper than that for the low-frequency mode at a given displacement. In addition to moving away faster, the wave packet will also return faster. The physically significant aspect of the dynamics is that the overlap rises faster in time and reaches its maximum faster for a high-frequency mode than for a low-frequency mode. Thus, at short

(18) The formula to convert the dimensionless displacement Δ into Å is

$$\delta = 10^8\Delta\sqrt{\frac{6.023\times10^{23}}{m}\,\frac{\hbar}{2\pi c\omega}}$$

where m is the mass involved in the vibration in molecular atomic mass, ω is the wavenumber of the vibrational mode in cm^{-1}, c is the speed of light in cm s^{-1}, δ is the displacement in Å, and Δ is the dimensionless displacement.

time the area under the overlap curve is larger for the high-frequency mode. After many recurrences, the areas under the curves are about the same for both modes.

When the damping factor is large (Figure 3c), the overlap of a high-frequency mode is still large but the overlap of a low-frequency mode is significantly damped out. Thus, for modes having similar displacements but different vibrational frequencies, the higher the frequency the greater the Raman intensity when the damping factor is large.

Effect of Γ. Short-time dynamics will dominate when (1) the damping factor, Γ, is large, (2) when several modes have significant displacements, and (3) when ω_1 is detuned just off resonance. In this section the damping factor, Γ, is discussed. The effect of other modes will be discussed in detail in section D. The previous two sections have shown that Raman intensities are intimately related to the damping factor. More specifically, they are related to the magnitude of the overlap as a function of time.

When Γ is large, the relative Raman intensities are dominated by the behavior of the wave packet at short times because long-time dynamics are damped out. This situation is common for large inorganic molecules in condensed media. A spectral signature is a smooth Raman excitation profile. When the damping factor is small, the wave packet will return to its origin many times, leading to many recurrences in the plot of overlap versus time. In this case, the excitation profiles will be structured and the relative intensities of the fundamentals will change dramatically as a function of the wave number of the incident radiation. In this section, explicit effects of Γ on the relative intensities are illustrated.

The functional form of the damping factor, $\exp(-\Gamma t)$, is an exponential decay. The time required for this function to decay to $1/e$ of its initial magnitude is given by[19]

$$t\ (\text{ps}) = 5.3/\Gamma\ (\text{cm}^{-1}) \qquad (4)$$

The time required for one vibration is 0.189 ps for the 176-cm^{-1} mode (ν_{10}), 0.115 ps for the 289-cm^{-1} mode (ν_1), 0.099 ps for the 338-cm^{-1} mode (ν_2), and 0.021 ps for the 1588-cm^{-1} mode (ν_9). When Γ is 10 cm^{-1}, the recurrence of even a low-frequency mode (176 cm^{-1}) is still relatively large. When Γ is 50 cm^{-1}, the recurrence of the 176-cm^{-1} mode (ν_1) is almost entirely damped out. However, the recurrences of the ν_1 and ν_2 modes are still significant. When Γ is 500 cm^{-1}, all of the recurrences are damped out and only the initial rise of the overlap is important.

Explicit effects of Γ on two modes having similar vibrational frequencies but significantly different displacements are shown in Figure 4. The magnitudes of the overlap for ν_1 (—) and ν_2 (-·-) versus time are shown in Figure 4a for a damping factor of 50 cm^{-1} and in Figure 4b for a damping factor of 300 cm^{-1}. When the damping factor is 50 cm^{-1}, the second peak in the overlap is not damped out. Thus, the profiles are highly structured and the relative intensity of ν_2 to ν_1 varies as a function of the wavenumber of the incident radiation. The excitation profiles for ν_1 (left) and ν_2 (right) for a damping factor of 50 cm^{-1} are shown in the inset to Figure 4a. When the damping factor is 300 cm^{-1}, the first peak in the overlap is somewhat decreased in magnitude but the other peaks are damped out. The magnitude of the first peak for ν_2 is much smaller than that for ν_1. Therefore, the Raman intensity of ν_2 relative to that of ν_1 is smaller than that calculated with a damping factor of 50 cm^{-1}. The resonance Raman excitation profiles for ν_1 (—) and ν_2 (-·-) with a damping factor of 300 cm^{-1} are shown in the inset to Figure 4b. When the damping factor is 300 cm^{-1} or larger, the reduction in the magnitude of the overlap for ν_1 and ν_2 is similar and the relative intensity of ν_2 to ν_1 does not change significantly.

When the difference in vibrational frequency between two modes is large and the displacements of these modes are the same (for example, ν_9 and ν_{10}), the effect of the damping factor on the Raman intensity is most pronounced on the lowest frequency mode. The magnitudes of the overlaps versus time for ν_9 (—) and ν_{10} (-·-) are shown in parts a and b, respectively, of Figure 3 when the damping factor is 100 cm^{-1}. The resonance Raman excitation profiles for these modes are shown in the inset to Figure 3a. Although the magnitude of the overlap for ν_{10} is reduced more than that for ν_9 because the overlap of ν_{10} increases more slowly than that of ν_9, the damping factor in this example is small enough to allow many recurrences in both modes. Thus, the relative Raman intensities of ν_{10} and ν_9 are comparable. When the damping factor is increased to 1000 cm^{-1}, only the first peak in the overlap survives. The overlaps for ν_9 (—) and ν_{10} (-·-) versus time are shown with an expanded time scale in Figure 3c. In this case, the magnitude of the overlap of ν_9 is much larger than that of ν_{10} because the overlap of ν_9 develops faster in time. The excitation profiles for ν_9 (—) and for ν_{10} (-·-) are shown in the inset to Figure 3c. The intensity of ν_{10} relative to that of ν_9 is greatly reduced compared to that when the damping factor is 100 cm^{-1}.

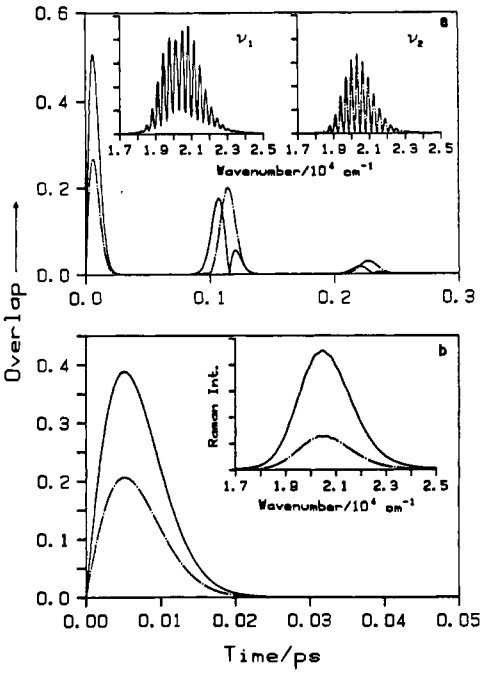

Figure 4. Magnitude of the overlap versus time for ν_1 (289 cm^{-1}, Δ = 3.73, —) and for ν_2 (338 cm^{-1}, Δ = 1.70, -·-) when the damping factor is (a) 50 cm^{-1} (inset on the left shows the excitation profile of ν_1 (—) when the damping factor is 50 cm^{-1} and E_{00} is 17 950 cm^{-1} and the inset on the right shows the excitation profile of ν_2 (-·-) when the damping factor is 50 cm^{-1} and E_{00} is 17 950 cm^{-1}) (b) 300 cm^{-1} (inset shows the excitation profiles of ν_1 (—) and ν_2 (-·-) when the damping factor is 300 cm^{-1} and E_{00} is 17 950 cm^{-1}).

The Γ dependence of the relative resonance Raman intensities of two modes is much more sensitive to their difference in frequency than to their difference in displacement. The reason for this dependence is found in the short-time dynamics of the wave packets, which is much more sensitive to the frequency at a given displacement than to the displacement for a given frequency. This simple physical picture provides an explanation for why very low frequency metal–ligand modes in a large molecule often do not appear in the resonance Raman spectrum even though the modes have appreciable displacements.

Another effect of a large damping factor is to "fill in" the excitation profiles, i.e., to give poorly resolved structure or a smooth envelope. When the damping factor is large enough to give a smooth envelope in the excitation profiles, the maxima of the excitation profiles of the fundamental and the overtone bands occur at about the same positions (vide infra).

The resonance Raman excitation profiles of different vibrational modes in the same molecule may have considerably different band shapes. To illustrate this result, the ratio of the resonance Raman intensity of ν_1 to that of ν_2 throughout the resonance region is shown in Figure 5. The solid line is for a damping factor of 50 cm^{-1}, and the dash-dotted line is for a damping factor of 300 cm^{-1}.

(19) $t = 1/(2\pi c\Gamma) = 5.3/\Gamma$ ps, where c is the speed of light and Γ is a damping factor in cm^{-1}.

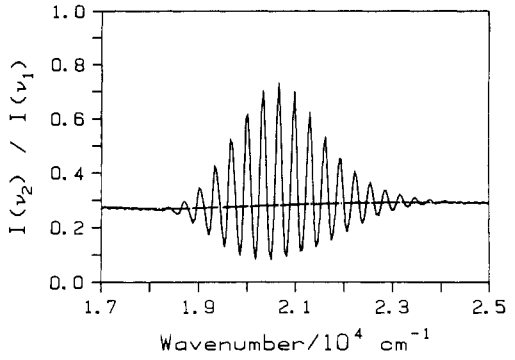

Figure 5. The ratio of the resonance Raman intensity of ν_1 to that of ν_2 throughout the resonance region for a damping factor of 50 cm^{-1} (—) and 300 cm^{-1} (-·-). ν_1 = 289 cm^{-1}, Δ_1 = 3.73, ν_2 = 338 cm^{-1}, Δ_2 = 1.70, and E_{00} = 17950 cm^{-1}.

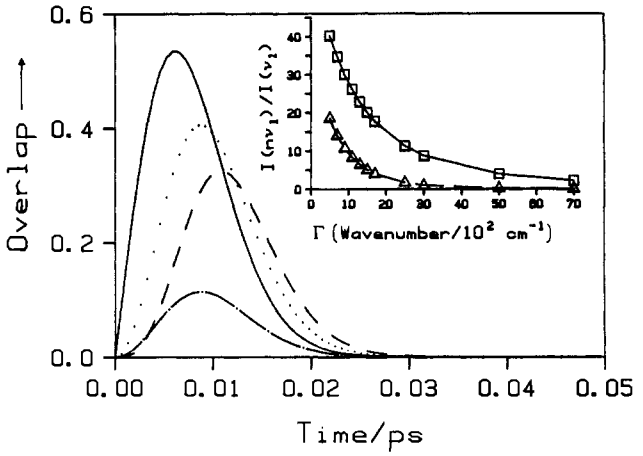

Figure 6. Magnitude of the overlaps versus time for ν_1 (—), $2\nu_1$ (···), $3\nu_1$ (---), and $2\nu_2$ (-·-). ν_1 = 289 cm^{-1}, Δ_1 = 3.73, ν_2 = 338 cm^{-1}, Δ_2 = 1.70, and Γ = 0. The inset shows the intensity ratio $I(n\nu_1)/I(\nu_1)$ versus the damping factor for n = 2 (squares) and for n = 3 (triangles).

When the damping factor is 50 cm^{-1}, the profiles are highly structured and the intensity ratio $I(\nu_2)/I(\nu_1)$ varies widely throughout the resonance region. When the damping factor is 300 cm^{-1}, the profiles are smooth and the intensity ratio $I(\nu_2)/I(\nu_1)$ is constant. In the latter case, Savin's formula[20]

$$\frac{I_k}{I_{k'}} = \frac{\Delta_k^2\omega_k^2}{\Delta_{k'}^2\omega_{k'}^2} \tag{5}$$

gives good estimates of the relative displacements of the modes from the relative intensities in the resonance Raman spectrum.

B. Overtone Bands. Effect of Δ. The reasons the vibrational modes that have the largest displacements are the most likely to have the largest overtone intensities in a resonance Raman spectrum are discussed in this section. The physical meaning of eq 1-3 is illustrated by the same two-mode example as was used to discuss the fundamentals (ν_1 = 289 cm^{-1}, Δ_1 = 3.73, ν_2 = 338 cm^{-1}, Δ_2 = 1.70). The first maxima of the overlaps of $n\nu_1$ (n = 1, 2, or 3) and $2\nu_2$ versus time are shown in Figure 6. A damping factor of zero was used to calculate the plots.

Consider first the relative intensities of the first overtones of ν_1 and ν_2 in Figure 6. The first maximum in the overlap is much larger and increases faster in time for the most highly displaced mode $2\nu_1$ (···) than that for the mode which has the lower displacement $2\nu_2$ (-·-). This trend is the same as that for the fundamentals. Thus, when Γ is large, the overlap of the highly displaced mode is damped less than that of the mode with a lower displacement and the overtone intensity is larger. The magnitudes of the recurrences after the first maximum are greater for $2\nu_2$ than for $2\nu_1$. Therefore, the Raman intensities of the overtone bands for the modes that have higher displacements are not necessarily higher than those for the modes that have lower displacements when Γ is small. However, the peaks after the first maximum are not important when the damping factor is large.

Consider next the relative intensities of the first and second overtones to that of the fundamental of a given mode. For example, the overlaps of $n\nu_1$ (n = 1, 2, or 3) are plotted in Figure 6. The magnitude of the first maximum decreases and in addition rises more slowly in time as the vibrational quantum number n increases. Therefore, the Raman intensities of the overtone bands relative to that of a fundamental decrease as n increases when the damping factor is large. However, when the damping factor is small and the excitation profiles are highly structured, there can be specific excitation wavelengths where the overtone intensities are higher than that of a fundamental.

Effect of Vibrational Frequency. The effect of vibrational frequency on the Raman intensities of overtone bands follows the same trend as its effect on the fundamentals. The higher the frequency, the faster the movement of the wave packet and the faster the development of appreciable overlap. When the damping factor is large, the overlap that occurs at short time dominates the Raman intensity. Therefore, the intensities of the overtone bands for a high-frequency mode are greater than those for a low-frequency mode when the displacements of both modes are the same.

Effect of Γ. The damping factor has the same general effect on the intensities of the overtone bands as it does on the fundamentals. As shown above, the first maximum in the overlap for overtone bands occurs later in time than that for a fundamental as n increases. The higher the quantum number, the slower the increase in the overlap and the later the occurrence of the first peak in the overlap. Therefore, the magnitudes of the overlaps for overtone bands suffer more reduction than that of a fundamental, leading to more reduction in the Raman intensity when the damping factor is increased. However, this reasoning will no longer be true if the damping factor is so small that many recurrences in the overlap take place.

The effect of the damping factor on the intensity ratio $I(n\nu_1)/I(\nu_1)$ (n = 2, 3) is shown in the inset to Figure 6. The intensities of the overtone bands decrease as the damping factor increases. The intensities of overtones relative to that of a fundamental decrease continuously as the damping factor increases.

The intensities of overtone bands of a low-frequency mode are affected more by an increase in the damping factor than those of a high-frequency mode. The reason is again found in the time development of the overlap. The initial increase of the overlap occurs more slowly and the maximum is found later in time for a low-frequency mode than for a high-frequency mode.

C. Combination Bands. Effect of Δ. The intensity of combination bands is explained by the magnitude of the overlap and by the time at which the overlap reaches its first maximum. The following discussion assumes that Γ is large. In general, the Raman intensity of any combination band $n\nu_1 + n'\nu_2$ is lower than that of the fundamentals of the modes contributing to it. The reason is that the magnitude of the first maximum and of the subsequent recurrences of the overlap for a combination band are much smaller than those of the fundamentals that are the components of the combination band.

The intensities of specific combination bands of the form $2\nu_1 + \nu_2$ (short dashed line in Figure 7a) and $\nu_1 + 2\nu_2$ (dotted line in Figure 7a) are governed by the magnitudes of the initial overlaps. If ν_1 has a larger displacement than ν_2, then the magnitude of the first maximum will be largest for $2\nu_1 + \nu_2$. For general progressions of the type $n\nu_a + n'\nu_b$, a large displacement of one of the partners will give rise to a more intense combination band progression. For example, if ν_a is the most highly displaced, the spectrum will contain a longer progression in $n\nu_a + \nu_b$ than in $\nu_a + n'\nu_b$. Within the series $n\nu_a + \nu_b$, the relative intensities of the members are governed by the time at which the overlap reaches its first maximum (Figure 7a). As n increases, the time at which the first maximum occurs increases and thus the relative intensities decrease.

(20) (a) Tang, J.; Albercht, A. C. In *Raman Spectroscopy*; Szynanski, H., Ed.; Plenum Press: New York, 1970; Vol. 2, p 33. (b) Warshel, A.; Dauber, P. *J. Chem. Phys.* **1977**, *66*, 5477.

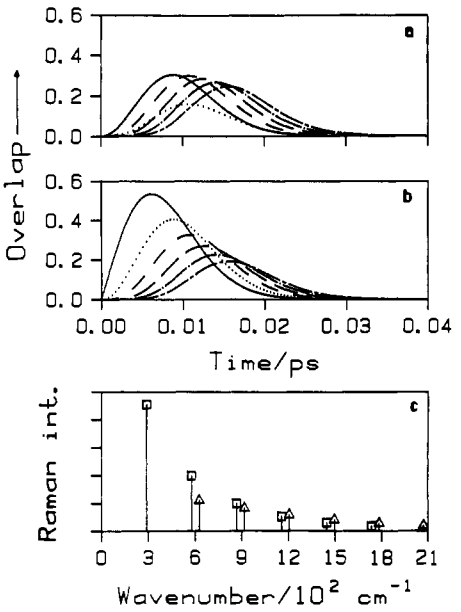

Figure 7. (a) Magnitudes of the overlaps versus time for $\nu_1 + \nu_2$ (—), $2\nu_1 + \nu_2$ (·--), $3\nu_1 + \nu_2$ (--), $4\nu_1 + \nu_2$ (-·-), $5\nu_1 + \nu_2$ (- -), and $\nu_1 + 2\nu_2$ (···), with ν_1 = 289 cm^{-1}, Δ_1 = 3.73, ν_2 = 338 cm^{-1}, Δ_2 = 1.70, and Γ = 0. (b) Magnitudes of overlaps versus time for ν_1 (—), $2\nu_1$ (···), $3\nu_1$ (---), $4\nu_1$ (--), $5\nu_1$ (-·-), $6\nu_1$ (- -), with ν_1 = 289 cm^{-1}, Δ_1 = 3.73, and Γ = 0. (c) Calculated resonance Raman spectra for $n\nu_1$ (squares) and $n\nu_1 + \nu_2$ (triangles), with ν_1 = 289 cm^{-1}, Δ_1 = 3.73, ν_2 = 338 cm^{-1}, Δ_2 = 1.70, Γ = 375 cm^{-1}, E_{00} = 17950 cm^{-1}, and ω_I = 20000 cm^{-1}.

Experimental resonance Raman spectra sometimes show a $(n-1)\nu_1 + \nu_2$ combination more intense than the $n\nu_1$ overtone bands at high values of n (n = 2, 3, ...).[21] The same two-mode example (ν_1 = 289 cm^{-1}, Δ_1 = 3.73, ν_2 = 338 cm^{-1}, Δ_2 = 1.70) is used to illustrate this phenomenon. The highly displaced ν_1 (289 cm^{-1}) mode is a progression-forming mode. The first maxima in the overlaps of $n\nu_1$ (n = 1–6), overtone bands, in the time domain are shown in Figure 7b, and those of $n\nu_1 + \nu_2$ (n = 2–5), combination bands, are shown in Figure 7a. A damping factor equal to zero was used in the plots. The magnitude of the first maximum in the overlap of the overtone band decreases more rapidly than that of the combination band. The first peak in the overlap of $3\nu_1$ is larger than that in the overlap of $2\nu_1 + \nu_2$. The maxima of these two peaks occur at about the same time. Therefore, the Raman intensity of $3\nu_1$ is larger than that of $2\nu_1 + \nu_2$ under a finite damping factor. However, the first peak in the overlap of $4\nu_1$ is smaller than that in the overlap of $3\nu_1 + \nu_2$. Therefore, the Raman intensity of $3\nu_1 + \nu_2$ is greater than that of $4\nu_1$. The calculated resonance Raman spectrum is shown in Figure 7c for the $n\nu_1$ and $n\nu_1 + \nu_2$ progressions. The intensity of the members of the $(n-1)\nu_1 + \nu_2$ progression is greater relative to those of the $n\nu_1$ progression when n is more than 4 in this example.

Effect of Vibrational Frequency. The effect of the vibrational frequency on the combination bands follows the same trends as its effect on fundamentals and overtone bands. The magnitude of the overlap for a given member in the combination progression coming from a high-frequency mode occurs faster in time than that from the corresponding member in a low-frequency mode. Therefore, the Raman intensities of the combination progression coming from a high-frequency mode are much greater than those from a low-frequency mode when the damping factor is large.

Effect of Γ. The damping factor has the same general effect on the intensities of combination bands as it does on fundamentals and overtone bands as discussed above. When Γ is large and the excitation profiles are smooth, short-time processes dominate and the simple trends discussed above are readily explained. When Γ is small, the intensities change dramatically as a function of the excitation wavenumber and no simple trends exist. However, the intensities can be readily calculated by using eq 1–3 and specific intensities can be compared on a case by case basis.

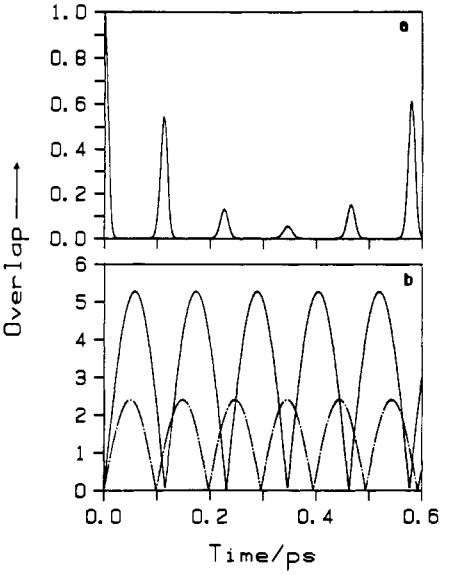

Figure 8. Overlap for (a) the absorption part (A) and (b) the Raman part (R) of eq 2 versus time for ν_1 (—) and for ν_2 (-·-), with ν_1 = 289 cm^{-1}, Δ_1 = 3.73, ν_2 = 338 cm^{-1}, Δ_2 = 1.70, and Γ = 0.

D. Relationship between Absorption Spectra and Resonance Raman Spectra. The expression for the total overlap in eq 2 is factored in a manner that emphasizes the relationship between the overlap governing the absorption spectrum and that governing the Raman spectra. The overlap $\langle\phi_f|\phi(t)\rangle$ is composed of two parts. The exponential term in brackets is the kernel of absorption (A) and the other term is the Raman factor (R). Each of these parts is discussed individually below in order to explicitly illustrate this relationship. In the example to be discussed, the displacement is 3.73 for ν_1 (289 cm^{-1}) and 1.70 for ν_2 (338 cm^{-1}). After these parts are examined, the reason multiple modes act as a damping factor is explained.

The overlap for the absorption part (A) versus time is shown in Figure 8a. The magnitude of the overlap is 1 at time zero. It decreases with time as the wave packets move away from their original positions. At later time as the wave packets come back to their original positions, it increases, giving a recurrence in the overlap. As the total displacement increases, the initial magnitude of the overlap falls off faster and the width of the spectrum increases. The full Fourier transform of the overlap gives the absorption spectrum. Because the moving wavepacket $\phi(t)$ is the same for the absorption and Raman processes, both spectroscopies can provide the same information about the molecule in the excited state. However, Raman spectroscopy is generally more useful. Unless the absorption spectrum is highly structured, Raman spectroscopy is the only way to obtain information about the individual normal coordinates because the profiles are the spectra filtered into the modes that are strongly coupled to the excited state in consideration.

The overlaps for the Raman part (R) for $1\nu_1$ (—) and $1\nu_2$ (-·-) are shown in Figure 8b. The initial increase of the magnitude of the Raman factor is the fastest in time for the most highly displaced mode. In addition, the overall magnitude is greatest for the mode that has the highest displacement. The Raman factor is zero at time zero. After one vibrational period, it goes to zero again. The product of the Raman and absorption parts is the total overlap for the Raman scattering that was extensively discussed in the previous sections. Note that the times at which the Raman factor reaches its maxima in Figure 8b are the same as those at which the absorption part is at its minima in Figure 8a. Therefore, the magnitude of the Raman factor at times close to the beginning and end of each vibrational period is important even though the magnitude at such times is not the maximum.

The effect of other modes on the intensity of a given fundamental, overtone, or combination band is readily explained in terms of the two parts of the total overlap. When other modes are

(21) Clark, R. J. H.; Ferris, L. T. H. *Inorg. Chem.* **1981**, *20*, 2759.

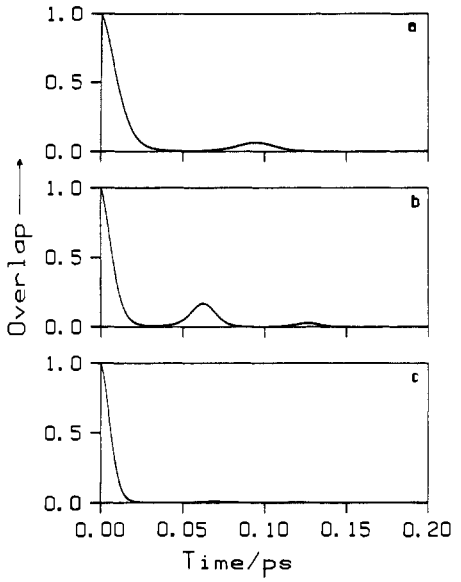

Figure 9. Overlap of the absorption part (A) of eq 2 versus time for (a) the 338-cm^{-1} mode ($\Delta = 2.0$, $\Gamma = 0$), (b) the 521-cm^{-1} mode ($\Delta = 2.0$, $\Gamma = 0$), and (c) the product of the two modes.

included in the calculation, only the absorption part is changed. The Raman factor stays the same for the particular mode under consideration. The other modes act as a damping factor on the absorption part and thus affect the Raman intensity of a given mode in a manner very similar to the effect of Γ.

To dramatically illustrate the effect of including additional modes in a calculation, two new modes, 338 cm^{-1} ($\Delta = 2.0$) and 521 cm^{-1} ($\Delta = 2.0$), are added. The absorption parts of the overlaps for these new modes are shown individually in parts a and b, respectively, of Figure 9. The recurrence of the overlap for the 338-cm^{-1} mode occurs between the recurrences of the overlap for the 521-cm^{-1} mode. Because the maxima from the first mode occur at the minima of the second, the product of the two overlaps will be smaller than either of the component overlaps as shown in Figure 9c. The net effect of these two modes is similar to that of the damping factor because the overlap is diminished at long times.

The product of the overlap in Figure 9c with the overlap of any given mode in a multimode calculation will reduce the overlap of the given mode at long times. Thus, the Raman intensity of a given mode will be decreased with the inclusion of the two new modes and any structure in the excitation profile will become less resolved. The exact magnitudes of these effects will depend on the frequencies and displacements of the new modes which are included, but the trends will be the same as those caused by increasing the damping factor.

4. Interpretation of Experimental Spectra

Two examples of the calculation of excited-state distortions from resonance Raman spectra are discussed below. These examples were chosen to illustrate the features that were discussed above and to present concrete examples of the power of the theory. The first example is the spectrum of $W(CO)_5(py)$, which contains only fundamentals. The second example consists of spectra of $Rh_2(O_2CCH_3)_4L_2$, where L = PPh_3 or $AsPh_3$, which contain smaller numbers of fundamentals but exhibit long overtone progressions and combination bands. The calculations for each molecule use one set of values of Δ_k, ω_k, ω_I, Γ, and E_{00}. E_{00} is determined from the emission spectrum for $W(CO)_5(py)$ and from the absorption spectrum for $Rh_2(O_2CCH_3)_4L_2$, where L = PPh_3 or $AsPh_3$, the ω_k's are determined from the Raman spectrum, and ω_I is the excitation wavenumber used to obtain the resonance Raman spectrum. The only variables are the Δ_k's and Γ. The single set of parameters defines one potential surface, which is used to calculate all of the excitation profiles for the fundamental, overtone, and combination bands and to calculate the resonance Raman spectrum at a given excitation wavelength.

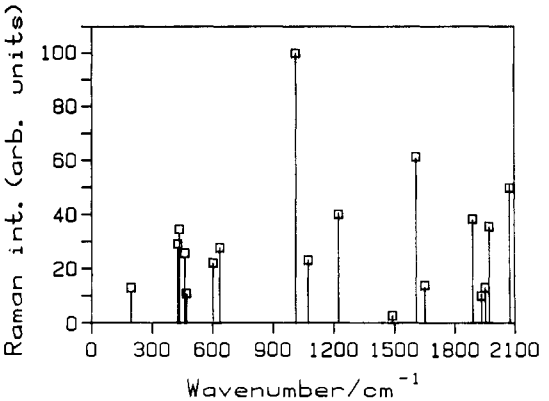

Figure 10. Calculated and experimental resonance Raman spectra of $W(CO)_5(py)$ at 476.5-nm excitation: (solid line) experimental intensities; (squares) calculated intensities.

Table I. Calculated Displacements for $W(CO)_5(py)$

ω_k, cm^{-1}	Δ_k (emission)[a]	Δ_k (Raman)[b]	ω_k, cm^{-1}	Δ_k (emission)[a]	Δ_k (Raman)[b]
2075	0.28	0.32	1073	0.37	0.37
1973	0.24	0.28	1012	0.81	0.81
1953	0.15	0.17	636	0.68	0.65
1934	0.14	0.15	602	0.64	0.61
1890	0.27	0.30	470	0.56	0.54
1651	0.18	0.20	462	0.87	0.85
1607	0.39	0.43	434	1.08	1.04
1489	0.10	0.10	427	1.01	0.97
1223	0.43	0.44	195	1.42	1.38

[a] Displacements used in ref 12. [b] Displacements are in dimensionless coordinates. E_{00} = 20 500 cm^{-1}, Γ = 6000 cm^{-1}, and ω_I = 4765 Å.

A. $W(CO)_5(py)$. This molecule has played an important role in inorganic spectroscopy because the missing-mode effect (MIME) was first recognized in its electronic emission spectrum. The MIME is a regularly spaced vibronic progression in the luminescence spectrum that does not correspond to any ground-state normal-mode vibration.[11-13,22] The MIME was quantitatively analyzed by using the resonance Raman intensities and eq 5 to calculate the distortions. A complete calculation of the Raman spectrum has not yet been attempted.

The resonance Raman spectrum of $W(CO)_5(py)$ is shown in Figure 10. The vertical lines are the integrated intensities of the peaks at the indicated wavenumbers in the experimental spectrum. Each of these 18 bands has been assigned to the fundamental of a normal mode. No overtone or combination bands are found. All of the bands having intensities greater than 0.01 of that of the most intense band in the spectrum are shown.

Two general features of the spectrum can be readily interpreted in terms of the aspects of the time-dependent theory discussed above. First, note the absence of overtones and combination bands. This absence is expected because the large number of displaced modes act as a damping factor. As was illustrated in Figure 9, when the maximum in the recurrence of the overlap of one mode happens at the same time that the overlap of a different mode is at a minimum, the product of the overlaps will be small. In this system with 18 displaced modes having wavenumbers ranging from 195 to 2075 cm^{-1}, the likelihood of the diminution of the total overlap is large. Thus, the overtone and combination bands whose own recurrences are found at times longer than those of the fundamentals will be effectively damped out. Second, note that the intensities of the low-frequency modes are in general smaller than those of the higher frequency modes. Again, this effect is caused by the large number of modes acting as a damping factor. The initial development of the overlap is slower for the lower frequency modes. Thus, their intensities are in general lower even though their displacements are larger (vide infra).

(22) Preston, D. M.; Günter, W.; Lechner, A.; Gliemann, G.; Zink, J. I. *J. Am. Chem. Soc.* **1988**, *110*, 5628.

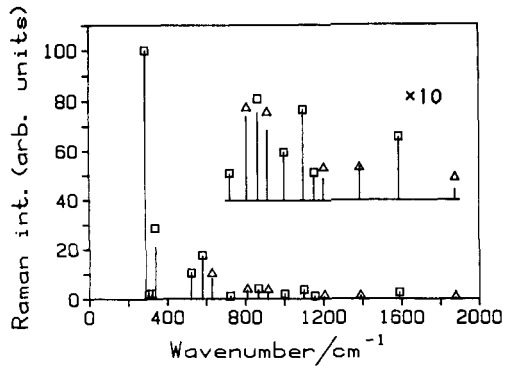

Figure 11. Calculated and experimental resonance Raman spectra of $Rh_2(O_2CCH_3)_4(PPh_3)_2$ at 356.4-nm excitation: (solid line) experimental intensities; (squares and triangles) calculated intensities.

Table II. Calculated Displacements for $Rh_2(O_2CCH_3)_4(PPh_3)_2$

ω_k, cm^{-1}	assignt	Δ_k[a]	ω_k, cm^{-1}	assignt	Δ_k[a]
289	ν_1(Rh–Rh)	3.73	725	δ(OCO)	0.15
305	Rh–O	0.51	1001	p-ring	0.14
320	Rh–O	0.48	1099	q X-sens	0.17
338	ν_2(Rh–O)	1.70	1588	k ν(C–C)	0.10
521	y X-sens	0.65			

[a] The Δ_k's are the displacements in dimensionless coordinates. Γ = 1350 cm^{-1}, ω_I = 356.4 nm, and E_{00} = 23 400 cm^{-1} (obtained from the electronic absorption spectrum).

The complete resonance Raman spectrum of $W(CO)_5(py)$ is calculated by using the parameters in Table I. The calculated intensities (represented by squares) for all 18 of the observed fundamental bands at the excitation wavelength 476.5 nm (ω_I = 20 986 cm^{-1}) are compared to those in the experimental resonance Raman spectrum in Figure 10. The calculated resonance Raman intensities are in excellent agreement with those in the experimental spectrum.

The displacements of all of the vibrational modes used in this calculation are compared to those used in the calculation of the MIME by Tutt, Tannor, et al.[12] in Table I. The values are very close to each other. The damping factor used in the calculation of the Raman intensities is larger than that used to calculate the emission spectrum because the Raman spectrum was taken at room temperature, while the emission spectrum was taken at 10 K.

B. Application to $Rh_2(O_2CCH_3)_4(PPh_3)_2$ and $Rh_2(O_2CCH_3)_4(AsPh_3)_2$. The spectra of $Rh_2(O_2CCH_3)_4(PPh_3)_2$ and $Rh_2(O_2CCH_3)_4(AsPh_3)_2$ offer an informative contrast to that of the tungsten compound treated above. In these cases the spectra are dominated by only two modes with relatively large displacements.[17,23] Many of the lines in the rich resonance Raman spectrum arise from overtones and combination bands involving the two most highly displaced modes.

The calculated intensities for all of the observed fundamental, overtone, and combination bands for $Rh_2(O_2CCH_3)_4(PPh_3)_2$ whose intensities are greater than 0.01 that of the most intense line are compared to those in the experimental spectrum in Figure 11. They are calculated by using the parameters given in Table II. The experimental Raman intensities are represented by vertical solid lines, and the calculated intensities are represented by squares and triangles. The calculated resonance Raman intensities are in excellent agreement with those in the experimental spectrum.

The excitation profiles of best fit (smooth lines) for the fundamentals ν_1 (ν(Rh–Rh)) and ν_2 (ν(Rh–O)), the overtone $2\nu_1$, and the combination band $\nu_1 + \nu_2$ of $Rh_2(O_2CCH_3)_4(PPh_3)_2$ are compared with the experimental data in Figure 12. The calculated and experimental excitation profiles are in excellent agreement. Not only is the experimental bandwidth and band shape of each excitation profile reproduced in the calculation but

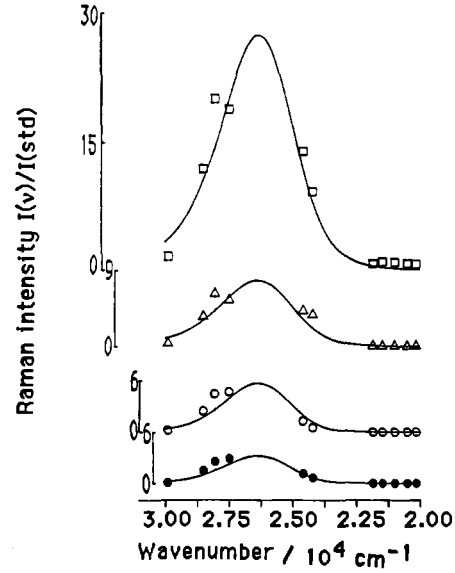

Figure 12. Calculated and experimental resonance Raman excitation profiles for ν_1 (□), ν_2 (△), $2\nu_1$ (○), and $\nu_1 + \nu_2$ (●) of $Rh_2(O_2CCH_3)_4(PPh_3)_2$.

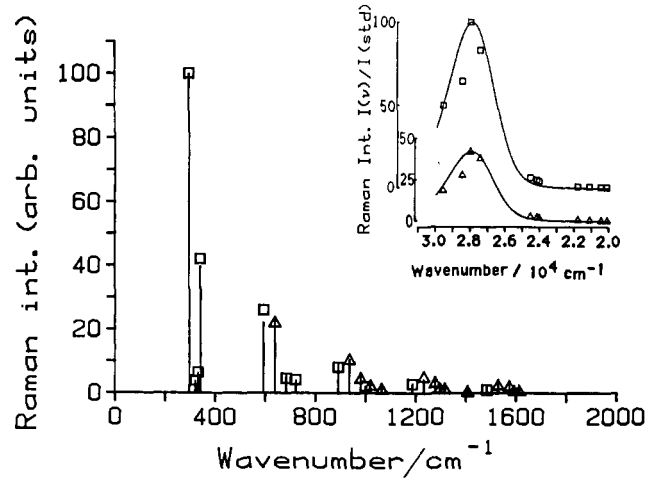

Figure 13. Calculated and experimental resonance Raman spectra of $Rh_2(O_2CCH_3)_4(AsPh_3)_2$ at 350.7-nm excitation: (solid line) experimental intensities; (squares and triangles) calculated intensities. The inset shows the calculated and experimental resonance Raman excitation profiles for ν_1 (□) and ν_2 (△).

also the relative intensities between each profile are reproduced as well. All calculated excitation profiles are normalized to the maximum of the ν_1 band. The maxima of all of the calculated excitation profiles are at 26 400 cm^{-1}, which corresponds to the maximum of the electronic absorption band with which the laser line is in resonance. The set of cross sections of excitation profiles for all modes at a given laser wavelength forms the resonance Raman spectrum.

The absorption spectrum can also be calculated by using the same parameters that were used to calculate the excitation profiles. The calculated full width at half-maximum and the peak maximum are 3980 and 26 200 cm^{-1}, respectively. The experimentally observed values are 3960 and 26 595 cm^{-1}, respectively.

The plots of the overlaps versus time in the time domain for each of the modes for $Rh_2(O_2CCH_3)_4(PPh_3)_2$ do not have any significant recurrences. The damping factor is large enough to damp out all the recurrences, and the wave packet never returns to its original position after it moves away from the Franck–Condon region.

The same type of calculation of the resonance Raman spectrum and the excitation profiles of $Rh_2(O_2CCH_3)_4(AsPh_3)_2$ further demonstrates the applicability of the theory. The calculated and experimental resonance Raman spectra for $Rh_2(O_2CCH_3)_4(AsPh_3)_2$ are shown in Figure 13. The excitation profiles of best

(23) Shin, K. S.; Clark, R. J. H.; Zink, J. I. *J. Am. Chem. Soc.* **1989**, *111*, 4244.

fit (smooth lines) for the two most highly displaced modes, ν_1, and ν_2, are shown in the inset of Figure 13.

In the process of excitation into the lowest allowed electronic transition of $Rh_2(O_2CCH_3)_4L_2$, where L = PPh_3 or $AsPh_3$, the largest bond length changes occur along the Rh-Rh and Rh-O bonds. The Rh-Rh bond length change in $Rh_2(O_2CCH_3)_4L_2$ is 0.047 Å for L = PPh_3 and 0.042 Å for L = $AsPh_3$. The Rh-O bond length change in $Rh_2(O_2CCH_3)_4L_2$ is 0.035 Å for L = PPh_3 and 0.041 Å for L = $AsPh_3$. There are also many modes that show small bond length or angle changes upon this excitation: for example, the C-O-C angle bend and the modes primarily involving phenyl rings. The O-C-O bond angle change in $Rh_2(O_2CCH_3)_4L_2$ is 0.46° for L = PPh_3 and 0.92° for L = $AsPh_3$. The magnitude of the change in the Rh-O bond on transition to an electronic state that is considered to be σ^*(Rh-Rh) is surprising. However, the metal d_{z^2} orbital which is the major component of the Rh-Rh σ interaction is also σ antibonding with respect to the oxygen atoms. Therefore, the $\sigma \rightarrow \sigma^*$ transition would be expected to change the net Rh-O bond and thus cause the displacement of the ν(Rh-O) normal coordinate. In addition, the significant displacement suggests that the resonant transition must also have RhO character to it, presumably via π(RhO) $\leftarrow d_{xy}$, π(RhO) $\leftarrow d_{xz}$, d_{yz}, and σ(RhO) $\leftarrow d_{z^2}$ parentage.

5. Summary

From the time-dependent point of view, the Raman intensities are governed by the overlap of the time-dependent wave packet with the final Raman wave function of interest as a function of time. The critical physical factors are the magnitude of the overlap and the time development of the overlap. The magnitude of the overlap for a fundamental is larger than that for overtones. The magnitude of a combination band is smaller than those of the fundamentals of the modes comprising the combination band. The time development of the overlap depends on both the frequency of the vibration and the displacement of the potential surface along the normal coordinate. The higher the frequency or the greater the displacement, the faster the time development. The overlaps of fundamentals develop faster in time than those of overtones. The damping of the overlap determines whether short-time or long-time processes dominate the intensities. For large molecules where short-time processes dominate, the larger the initial overlap and the faster the overlap increases with time, the higher the Raman intensity.

The resonance Raman spectrum of $W(CO)_5(py)$ was calculated. The calculated displacements are in excellent agreement with those determined in the analysis of the MIME. Both the excitation profiles and the resonance Raman spectra of $Rh_2(O_2CCH_3)_4L_2$, where L = PPh_3 or $AsPh_3$, have been accurately calculated. These molecules have significant displacements in the Rh-Rh and Rh-O normal coordinates.

Acknowledgment. This work was made possible by a grant from the National Science Foundation (CHE88-06775).

Contribution from the Department of Chemistry,
Northern Illinois University, DeKalb, Illinois 60115

Electronic Absorption and MCD Spectra for the Binuclear Three-Coordinate Gold(I) Complex $Au_2(dmpm)_3^{2+}$ (dmpm = Bis(dimethylphosphino)methane)

Huey-Rong C. Jaw, M. Meral Savas, and W. Roy Mason*

Received February 22, 1989

Electronic absorption and magnetic circular dichroism (MCD) spectra are reported for $[Au_2(dmpm)_3](ClO_4)_2$ in H_2O and CH_3CN solution in the region 2.5-5.2 μm^{-1}. Thin-film absorption spectra at 300 and 77 K are also reported for $[Au_2(dmpm)_3]Cl_2$ dissolved in polymerized poly(vinyl alcohol) (PVA). An intense band observed at 3.91 μm^{-1} is assigned as the Au_2-localized $d\sigma^* \rightarrow p\sigma$ transition of predominantly singlet character. The equivalent MCD band is weak and poorly resolved, a result that is interpreted in terms of orbital symmetry restrictions on the magnetic mixing of the excited state with close-lying states (*B*-term interactions). Two weaker bands to the red side of the spectrum are assigned to transitions to $d\sigma^* \rightarrow p\sigma$ and $d\delta \rightarrow p\sigma$ spin-orbit states of triplet parentage. At higher energy two poorly resolved intense bands are observed characterized by a strong positive *A* term in the MCD spectrum near 5.1 μm^{-1}. These bands are interpreted as due to transitions localized mainly within the AuP_3 unit. The spectroscopic results are compared with studies of related complexes.

Introduction

The binuclear gold(I) cation $Au_2(dmpm)_3^{2+}$ (dmpm = bis(dimethylphosphino)methane) has an interesting trigonal structure that consists of two nearly planar AuP_3 units linked by bridging dmpm ligands in a parallel face to face configuration. The Au-Au vector lies along the molecular C_3 axis and features a relatively short Au-Au distance (3.050 (1) Å in the BF_4^- salt).[1] The closed-shell $5d^{10}$-$5d^{10}$ electron configuration is formally nonbonding between the Au(I) ions, but the close Au-Au contact compared to the van der Waals distance (~3.4 Å)[2] indicates a significant Au-Au interaction. Short Au-Au contacts are found in other binuclear Au(I) complexes,[3,4] including the related $Au_2(dmpm)_2^{2+}$ cation (two linear AuP_2 units bridged parallel to one another with Au-Au = 3.028 (2) Å), which has been investigated extensively in our laboratory recently. The trigonal three-coordination of the Au(I) ions in the $Au_2(dmpm)_3^{2+}$ cation is less common than the linear two-coordination of $Au_2(dmpm)_2^{2+}$ and is believed to be responsible for several differences in their electronic absorption and magnetic circular dichroism (MCD) spectra in the UV region.[5] These features together with a recent report[6] of electronic spectra for the structurally similar nd^{10}-nd^{10} binuclear complexes $M_2(dppm)_3$ (M = Pd(0), Pt(0); dppm = bis(diphenylphosphino)methane) provided motivation for the present report of our spectroscopic studies of the $Au_2(dmpm)_3^{2+}$ cation. This paper reports room-temperature solution absorption and MCD spectra for $[Au_2(dmpm)_3](ClO_4)_2$ in water and acetonitrile in the region 2.5-5.2 μm^{-1} and absorption spectra for $[Au_2(dmpm)_3]Cl_2$ at 300 and 77 K in thin films of solid poly(vinyl alcohol) (PVA).

Experimental Section

Preparation of $Au_2(dmpm)_3^{2+}$ Salts. Bis(dimethylphosphino)methane, $(CH_3)_2PCH_2P(CH_3)_2$, was purchased from Strem Chemicals Co. and

(1) Bensch, W.; Prelati, M.; Ludwig, W. *J. Chem. Soc., Chem. Commun.* **1986**, 1762.
(2) Bondi, A. *J. Phys. Chem.* **1964**, *68*, 441.
(3) Puddephatt, R. J. *Comprehensive Coordination Chemistry*; Wilkinson, G., Gillard, R. D., McCleverty, J. A., Eds.; Pergamon Press: Oxford, England, 1987; Vol. 5, p 861.
(4) Jaw, H.-R. C.; Savas, M. M.; Rogers, R. D.; Mason, W. R. *Inorg. Chem.* **1989**, *28*, 1028 and references therein.
(5) Savas, M. M. Dissertation, Northern Illinois University, 1987.
(6) Harvey, P. D.; Gray, H. B. *J. Am. Chem. Soc.* **1988**, *110*, 2145.

0020-1669/89/1328-4366$01.50/0